

Direct numerical simulation of separated flow in a three-dimensional diffuser

JOHAN OHLSSON¹†, PHILIPP SCHLATTER¹,
PAUL F. FISCHER² AND DAN S. HENNINGSON¹

¹Linné Flow Centre, KTH Mechanics, Osquars Backe 18, SE-100 44 Stockholm, Sweden

²MCS, Argonne National Laboratory, 9700 S. Cass Avenue, Argonne, IL 60439, USA

(Received 13 October 2009; revised 28 January 2010; accepted 29 January 2010;
first published online 19 March 2010)

A direct numerical simulation (DNS) of turbulent flow in a three-dimensional diffuser at $Re = 10\,000$ (based on bulk velocity and inflow-duct height) was performed with a massively parallel high-order spectral element method running on up to 32 768 processors. Accurate inflow condition is ensured through unsteady trip forcing and a long development section. Mean flow results are in good agreement with experimental data by Cherry *et al.* (*Intl J. Heat Fluid Flow*, vol. 29, 2008, pp. 803–811), in particular the separated region starting from one corner and gradually spreading to the top expanding diffuser wall. It is found that the corner vortices induced by the secondary flow in the duct persist into the diffuser, where they give rise to a dominant low-speed streak, due to a similar mechanism as the ‘lift-up effect’ in transitional shear flows, thus governing the separation behaviour. Well-resolved simulations of complex turbulent flows are thus possible even at realistic Reynolds numbers, providing accurate and detailed information about the flow physics. The available Reynolds stress budgets provide valuable references for future development of turbulence models.

1. Introduction

In many engineering flows, such as the flow over airplane wings or in turbomachinery applications, flow separation may lead to degradation of lift, pressure losses, ‘hot spots’ or even engine failure. On the other hand, maximum performance is often obtained close to separation, hence the design of flow devices such as pumps, fans and compressors inevitably leads to situations where flow separation is necessary to predict, see e.g. the review article by Simpson (1989). In practical situations these flows are generally turbulent and fully three-dimensional, hence prediction of highly unsteady, three-dimensional separation is of considerable importance. Often separation is caused by an adverse pressure gradient and may take place over a smooth surface (‘pressure-induced’ separation), as opposed to the case where the flow separates from a sharp geometrical obstacle (‘geometry-induced’ separation). Since, in the latter case the separation point, in principle, is given by the point of highest curvature and is thus easy to predict, the former poses most uncertainties because the point of separation can vary in both time and space.

Rapid developments in computer hardware over the last few years allow predictions of complex flows to be made by numerical simulations. The most widely used

† Email address for correspondence: johan@mech.kth.se

approach for complex engineering flows is based on the Reynolds-averaged Navier–Stokes equations (RANS), where an ensemble average of the Navier–Stokes equations is solved for. The averaging process gives rise to an unclosed term, which has to be modelled. Although RANS may be a rather crude way to describe a highly time-dependent flow phenomenon, it may, in many situations, be sufficient to know the mean flow characteristics. However, flows experiencing adverse pressure gradients and separation are very hard to predict, in particular three-dimensional flows, due to rapid changes in mean flow properties (e.g. Jakirlić *et al.* 2010). For a more detailed picture of the flow, unsteadiness needs to be taken into account. The concept of large-eddy simulation (LES), where the large scales of the flow are resolved and the small scales are modelled by a subgrid-stress (SGS) model, has in recent years evolved into a promising tool for flow predictions. The drawback, however, is that a SGS model can never be universal, and special care has to be taken as new flow cases are being studied. A numerically more appealing approach and also the most computationally expensive, where the governing equations are solved without averaging or filtering, is referred to as direct numerical simulation (DNS). If proper boundary conditions are imposed and high-enough resolution is used, this approach generally compares very well to experimental data. Numerical schemes of high order, e.g. spectral methods, with low amounts of numerical viscosity and dispersion yield particularly satisfactory results. While traditional spectral methods only work efficiently for simple geometries, the spectral-element method (SEM) introduced by Patera (1984), is a high-order numerical method with the ability to accurately simulate fluid flows also in complex geometries. Thus, SEM has opened the possibility to study, in great detail, fluid phenomena known to be very sensitive to discretization errors, e.g. flows undergoing pressure-induced separation (Ohlsson *et al.* 2010). SEM has successfully been applied to mainly laminar and transitional flows (e.g. Sherwin & Karniadakis 1995; Tomboulides & Orszag 2000; Tufo & Fischer 2001) and also fully turbulent flows (Iliescu & Fischer 2003; Wasberg *et al.* 2009).

Pressure-induced separation has been considered extensively in two-dimensional flow configurations, where the mean flow exhibits one homogeneous direction, e.g. Kaltenbach *et al.* (1999) who performed LES of a plane asymmetric diffuser with 10° opening angle, experimentally also investigated by Buice & Eaton (2000). Herbst, Schlatter & Henningson (2007) performed LES of a plane asymmetric diffuser with 8.5° opening angle at higher Reynolds numbers. They all reported satisfactory agreement with the corresponding experimental data concerning the bulk quantities. Herbst *et al.* (2007), however, found that employing a recycling technique to specify unsteady turbulent inflow conditions may not be optimal for spatially developing flows exhibiting pressure-induced separation, since it might trigger artificial frequencies. Few examples of LES of fully three-dimensional, turbulent, pressure-induced separated flows are found in the literature (Schneider, Terzi & Rodi 2009) mainly due to the fact that one has to rely solely on one homogeneous direction, time, to average turbulent statistics.

Even though RANS models are getting more sophisticated, many difficulties remain among which some have already been pointed out. In order to continue the development, there is a need for clearly-defined benchmark cases and good quality reference data. Recently, experiments of such a reference case were performed by Cherry *et al.* The experiments conducted consisted of two three-dimensional diffusers with slightly different expansion angles at, for simulation standards, a fairly high yet realistic Reynolds number of 10 000 based on bulk velocity and height of the inflow duct. It was found that the flow was extremely sensitive to these slight changes in the

geometrical set-up. Magnetic resonance velocimetry (MRV) (see Elkins *et al.* 2003) was used to collect three-dimensional velocity data. Emphasis was put on defining a simple truly three-dimensional geometry with well-defined boundary conditions (walls), inlet conditions (fully developed turbulence) and to avoid any symmetries leading to long-period stall switches, hence facilitating for simulations to mimic the real experiment. The three-dimensionality was reasoned to be a more relevant test case for computational fluid dynamics (CFD), but it would also get rid of the ambiguities a two-dimensional experiment may suffer from, such as dependence on channel width. Here, we present a DNS of one of the diffuser cases ('Diffuser 1') in Cherry, Elkins & Eaton (2008) at the same Reynolds number as in the experiments. Focus is on accuracy, both in terms of discretization and boundary conditions. The motivation for this is twofold: first, we are aiming at understanding the flow physics involved in three-dimensional separation through a study of mean flow features together with the identification of instantaneous flow structures. Second, our data could be used as an important reference, suitable for further development of turbulence models. A first step towards these goals must be to validate the data against existing experimental data. Here, we focus on careful analysis of mean flow results in order to assess the quality of the simulation data. Mean flow, pressure recovery and turbulent fluctuations are compared to the experimental data of Cherry *et al.* (2008). Further, a brief discussion will be given on some of the new flow physics found in the diffuser.

2. Numerical method and simulation set-up

The incompressible Navier–Stokes equations are solved using a Legendre-polynomial-based spectral-element method, implemented in the code nek5000, developed by Fischer *et al.* (2008). As in the case of the finite-element method (FEM), the governing equations are cast into weak form and discretized in space by the Galerkin approximation, where the test and trial spaces are restricted to certain (and different) velocity and pressure spaces, respectively, following the $\mathbb{P}_N - \mathbb{P}_{N-2}$ SEM discretization by Maday & Patera (1989). The velocity space is typically a space of N th-order Lagrange polynomial interpolants, $h_i^N(x)$, based on tensor-product arrays of Gauss–Lobatto–Legendre (GLL) quadrature points in a local element, Ω^e , $e = 1, \dots, E$, satisfying $h_i^N(\xi_j^N) = \delta_{ij}$. Here, $\xi_j^N \in [-1, 1]$ denotes one of the $N + 1$ GLL quadrature points and δ_{ij} is the Kronecker delta. For a single element in \mathbb{R}^3 the representation of the velocity vector, \mathbf{u} , is

$$\mathbf{u}(\mathbf{x}^e(r, s, t))|_{\Omega^e} = \sum_{i=0}^N \sum_{j=0}^N \sum_{k=0}^N \mathbf{u}_{ijk}^e h_i^N(r) h_j^N(s) h_k^N(t), \quad (2.1)$$

where \mathbf{x}^e is the coordinate mapping from the reference element $\hat{\Omega}$ to the local element Ω^e and \mathbf{u}_{ijk}^e is the nodal basis coefficient. The tensor-product structure enables the use of highly optimized matrix–matrix routines (mxm) to solve the final system of equations (see e.g. Fischer 1997). The nonlinear terms are treated explicitly by second-order extrapolation (EXT2), whereas the viscous terms are treated implicitly by a second-order backward differentiation scheme (BDF2) leading to a linear symmetric Stokes system for the basis coefficient vectors $\underline{\mathbf{u}}^n$ and $\underline{\mathbf{p}}^n$ to be solved at every time step:

$$H \underline{\mathbf{u}}^n - D^T \underline{\mathbf{p}}^n = B \underline{\mathbf{f}}^n, \quad D \underline{\mathbf{u}}^n = 0. \quad (2.2)$$

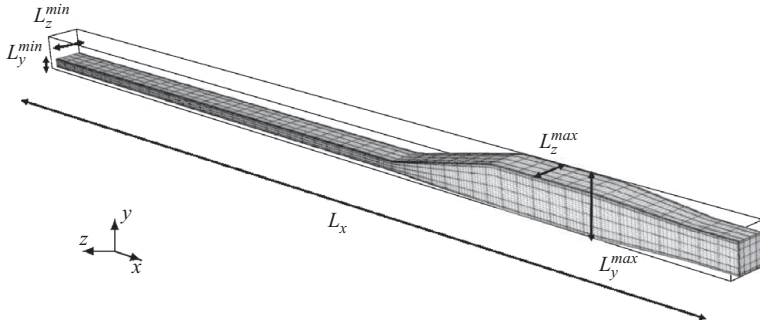


FIGURE 1. Grid of one of the diffuser geometries ('Diffuser 1') in Cherry *et al.* (2008) showing the development region, diffuser expansion, converging section and outlet.

Here, $H = (1/Re)K + (3/2\Delta t)B$ is the discrete equivalent of the Helmholtz operator $(-(1/Re)\nabla^2 + 3/2\Delta t)$. In the right-hand side, \underline{f}^n accounts for the nonlinear terms and for the cases we have external forcing in the Navier–Stokes equations. To solve the final problem (see (2.2)), velocity and pressure are decoupled and solved iteratively using conjugate gradients and GMRES with scalable Jacobi and additive Schwarz preconditioners, respectively (Fischer 1997). For the latter, fast parallel coarse-grid solvers scaling to ten thousands of processors are used (Tufo & Fischer 2001).

The computational domain shown in figure 1 is set up in close agreement with the diffuser geometry in the experiment and consists of the inflow development duct of almost 63 duct heights, h , (starting at the non-dimensional coordinate $x = -62.9$), the diffuser expansion located at $x = 0$ and the converging section upstream of the outlet. The corners resulting from the diffuser expansion are smoothly rounded with a radius of 6.0 in accordance with the experimental set-up. The maximum dimensions are $L_x = 105.4h$, $L_y = [h, 4h]$, $L_z = [3.33h, 4h]$. In the inflow duct, laminar flow undergoes natural transition by the use of an unsteady trip forcing (see e.g. Schlatter *et al.* 2009), which avoids the use of artificial turbulence and eliminates artificial temporal frequencies which may arise from inflow recycling methods (Herbst *et al.* 2007). A 'sponge region' is added at the end of the contraction in order to smoothly damp out turbulent fluctuations, thereby eliminating spurious pressure waves. It is followed by a homogeneous Dirichlet condition for the pressure and a homogeneous Neumann condition for the velocities. The resolution of approximately 220 million grid points is obtained by a total of 127 750 local tensor product domains (elements) with a polynomial order of 11, respectively, resulting in $\Delta z_{max}^+ \approx 11.6$, $\Delta y_{max}^+ \approx 13.2$ and $\Delta x_{max}^+ \approx 19.5$ in the duct centre and the first grid point being located at $z^+ \approx 0.074$ and $y^+ \approx 0.37$, respectively. It was verified that the present resolution yields accurate results in turbulent channel flow simulations. In the diffuser, the grid is linearly stretched in both directions, but since the mean resolution requirements decreases with the velocity, which decreases linearly with the area expansion, the resolution in the entire domain will hence be satisfactory. The simulation was performed on the Blue Gene/P at ALCF, Argonne National Laboratory (32 768 cores and a total of 8 million core hours) and on the cluster 'Ekman' at PDC, Stockholm (2048 cores and a total of 4 million core hours). Thirteen flow-through times, $tu_b/L = 13$, based on bulk velocity, u_b , and diffuser length, $L = 15h$, were simulated in order to let the flow settle to an equilibrium state before turbulent statistics were collected over approximately $tu_b/L = 21$ additional flow-through times. The lack of homogeneous directions together with the fact that the flow showed pronounced instationarity with

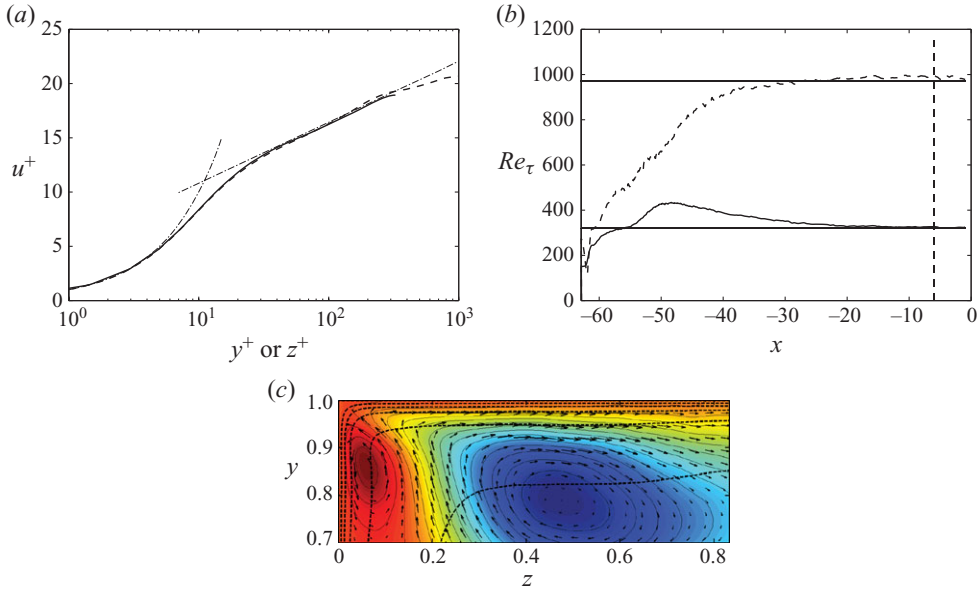


FIGURE 2. (a) Mean centerplane velocity profile $6h$ upstream of the diffuser throat, where — $u^+(y^+)$, --- $u^+(z^+)$, $\text{-}\cdot\text{-}$ log law with $\kappa=0.41$ and $B=5.2$, (b) evolution of $Re_{\tau,y} = u_{\tau,y}h/2\nu$ (—), $Re_{\tau,z} = u_{\tau,z}3.33h/2\nu$ (---) in a midplane of constant z and y , respectively, in the inflow section; solid horizontal lines showing Re_τ for a periodic duct and vertical dashed line location of the selected velocity profile in (a) and (c) stream function of the time-averaged flow field in a cross-sectional plane $6h$ upstream of the diffuser throat showing the secondary flow in one of the corners. Contour lines of the stream function are spaced 2×10^{-4} units apart. Dashed contour lines, $0.2 u_{bulk}$ apart, of streamwise velocity as well as velocity vectors of mean crossflow velocities are superimposed.

fluctuations on a wide range of scales, called for long integration time in order to average the statistics.

3. Results

3.1. Inflow section

The inflow duct was studied in detail to ensure that a fully developed turbulent flow is reached at the end of the development section described in §2. Mean velocity profiles as a function of y^+ and z^+ , respectively, taken from a middle plane a short distance upstream of the diffuser opening are shown in figure 2(a). Here, y^+ and z^+ are the cross-stream directions in the duct normalized with the respective viscous length scale in that direction. It can be seen that the ‘law of the wall’ is captured with good accuracy. Monitoring the streamwise development of the friction Reynolds number, Re_τ , figure 2(b), provides a measure to detect where a fully turbulent flow is reached. Compared to the value obtained from a periodic duct simulation at the same Re (indicated by solid horizontal lines), this has occurred at $x > -15$ as shown by the dashed vertical line. The secondary flow in the corners of the duct shown in figure 2(c) also gives a good indication on the development of the flow and, although weak (a few per cent of u_b), is thought to be important for the correct separation behaviour (Cherry *et al.* 2008). From the measures listed above, we conclude that the flow has converged to a statistically stationary state well upstream of the diffuser throat.

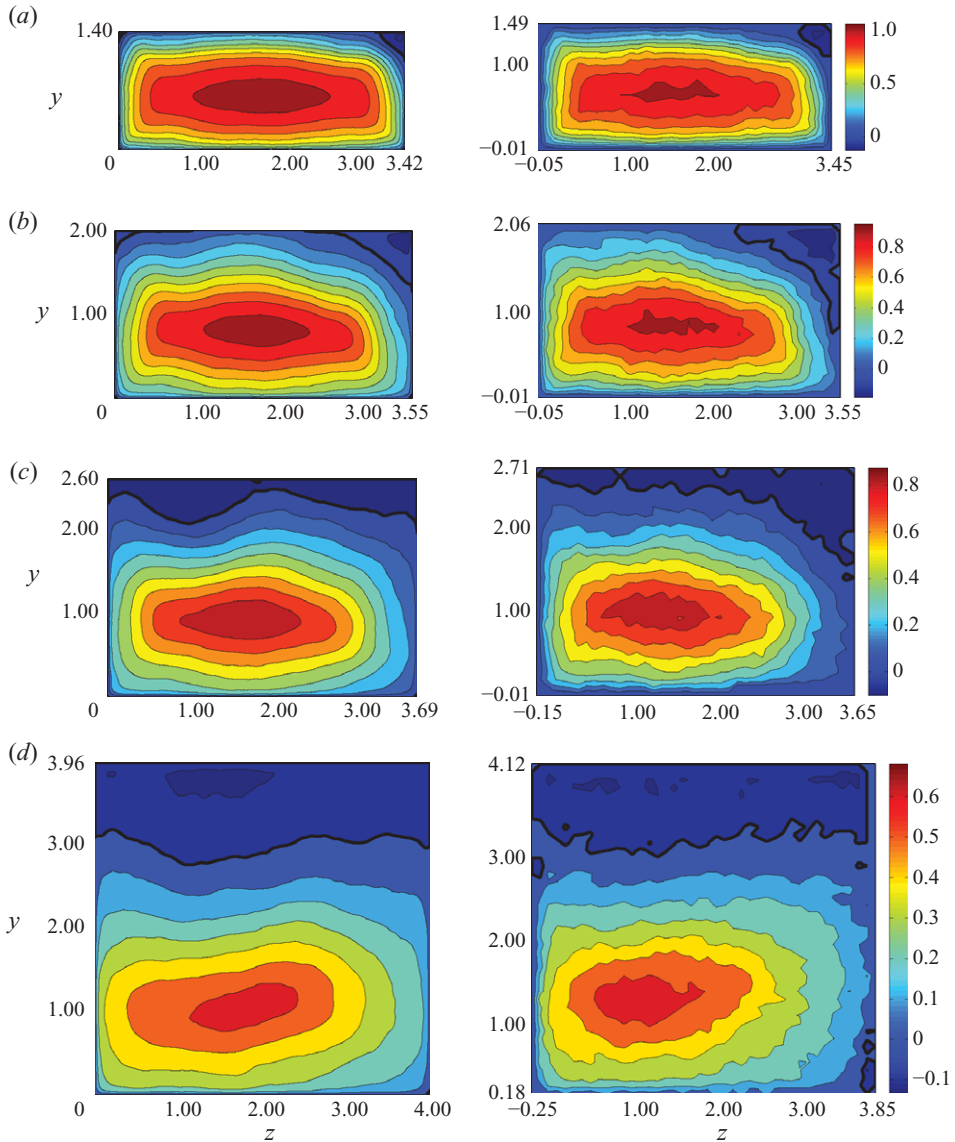


FIGURE 3. Crossflow planes of streamwise velocity 2, 5, 8 and 15 h downstream of the diffuser throat. *Left*: Computation by nek5000. *Right*: Experiment by Cherry *et al.* (2008). Each streamwise position has its own colour bar on the right. Contour lines are spaced $0.1 u_{bulk}$ apart. Thick black lines correspond to the zero velocity contour.

3.2. Diffuser

Turning to the flow in the actual diffuser, a qualitative analysis focusing on identifying the size, shape and location of the separated region is made by selecting a number of crossflow planes, shown in figure 3. At every location within the duct until the diffuser throat at $x=0$, there is no sign of separation, as expected. As soon as the diffuser starts to expand, the separation, as pointed out by Cherry *et al.* (2008), increases rapidly due to the asymmetry of the geometry in the uppermost right corner, where the two inclined walls meet. As can be seen in figure 3(a), at $x=2$, the agreement

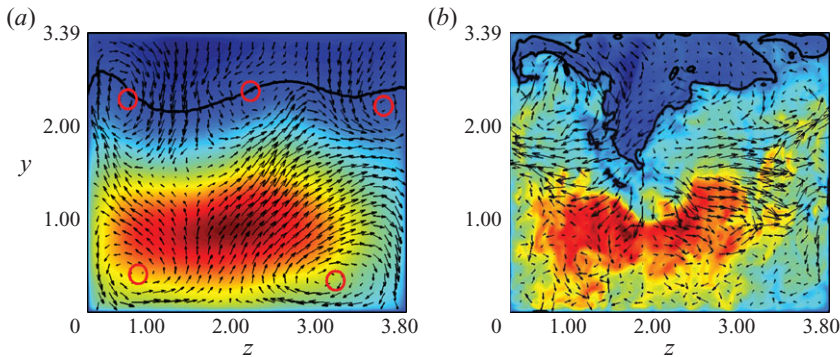


FIGURE 4. Crossflow planes of (a) mean and (b) instantaneous streamwise velocity 12 h downstream of the diffuser throat with superimposed crossflow vectors (scaled so that vectors in (a) are six times larger than vectors in (b)) showing the corner vortices responsible for the bump. Thick black lines correspond to the zero streamwise velocity contour. \circ refer to (primary) vortex centres.

between the experimental and simulation data is excellent, both considering the mean flow in general and the separated region in particular. Very good agreement between the simulation data and the experimental data persists for another three units downstream until $x = 5$, shown in figure 3(b), where the separation in the upper right corner gradually starts to spread and eventually includes the whole top wall of the diffuser. This spreading is present in both data sets, however, in slightly different ways. Studying figure 3(c) it is obvious that the separation in the experimental data advances like a wedge over to the top and uppermost left corner of the diffuser. (Note the slight shift of the coordinate system in the experimental data). The simulation data, on the other hand, indicates that at $x = 6$ (not shown) the smaller separation from the left corner visible in figure 3(b) has grown, although with fixed streamwise magnitude (~ -0.025), into a small, stretched localized region in the top of the diffuser. From here it rapidly continues to grow down into the interior of the diffuser, finally taking the shape of a small ‘bump’ hanging from the top wall at $x = 8$, figure 3(c). Here, the separation fills the entire top of the diffuser, consistent with the experiments. Even though the bump is not present at $x = 8$ in the experimental data, its presence can be noticed further downstream at $x = 15$ in figure 3(c), where the bulk of the separated flow indeed is located to the left. But even so, the origin of the discrepancy in figure 3(c) is at present unknown. It should be pointed out that the bump is not a transient effect and an artefact of a too short averaging time. Window averaging of the data has shown that it is present at all times. This is also confirmed by Schneider *et al.* (2009), who performed LES of the same diffuser geometry and Reynolds number and could see the same extension of the separation bubble on the top expanding wall. The physical reason for this particular behaviour becomes clear if we superimpose vectors of crossflow velocity onto a crossflow plane, as shown in figure 4. We see that a substantial downwash of slow velocity fluid is present within the bump, both in the mean (figure 4a) and instantaneously (figure 4b), governed by vortical structures in the upper corners. Tracking the secondary flow in the duct, one realizes that although weak in magnitude (a few per cent of the streamwise bulk velocity), the vortices produced by the secondary flow persist into the diffuser, where they give rise to a low-speed streak, because of a similar mechanism as the ‘lift-up effect’ in transitional shear flows (Landahl 1980). In the remaining part of the diffuser region, the area

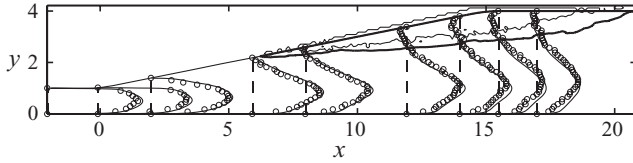


FIGURE 5. Mean centerplane velocity $3\langle u \rangle + x$ in the diffuser. Velocity data: — nek5000, \circ experiment by Cherry *et al.* (2008) Separated region: — nek5000, — experiment by Cherry *et al.* (2008).

fraction of separated flow (AFSF) in a cross-section is in very good agreement with the experimental data, including the maximum of 23 % AFSF occurring at $x = 15$, figure 3(d), where the straight part of the geometry begins. Between $x = 18$ –20 the AFSF is 2 % larger in the simulation data. After $x = 20$ the separation is reduced to zero, a result supported by both data sets. A more quantitative comparison is made in figure 5, where mean velocity profiles are selected in a spanwise midplane. Generally, good agreement is observed. In particular, the upward movement of the velocity peak is well captured. The presence of the large separated region on the upper inclined wall forces the flow upwards, however only slightly, due to the originally high momentum content in the flow. The size and location of the separated region (here defined as a region with negative velocity) in a spanwise midplane, seen in figure 5, is in good agreement with the experimental data, although the previously described extension of the separation in the simulation data is clearly visible. The streamwise root mean square (r.m.s), u_{rms}/u_b , given in figure 6 at the same streamwise locations as the mean flow in figure 3 shows consistency with the mean flow regarding the flow dynamics present in the diffuser. In front of the entrance to the diffuser the fluctuations peak ($u_{rms}^+ = 2.6$) close to the walls ($z^+ = 14.9$) very much like in a turbulent channel flow. The strong character of fully developed wall-bounded turbulence is further confirmed by the typical streak spacing of $\Delta z_{max}^+ \approx 100$ in the near-wall region. Shortly after the diffuser throat, the fluctuations generally move out from the walls. In particular, the most dominant fluctuations are found in the shear layer bounding the separation bubble in the uppermost right corner (figure 6a), reaching a magnitude of 22 % of the bulk inlet velocity, also confirmed by the experimental data. Further downstream, at $x = 5$ (figure 6b), the peak moves downward and increases in magnitude (up to 25 % of the bulk inlet velocity), indicating an intense turbulence activity in this area. At $x = 8$ (figure 6c) the turbulent shear layer follows consistently the spreading of the separation to the top wall of the diffuser, clearly seen in both data sets. The localized bump present in the simulation data has a corresponding enhanced turbulent activity around $(z, y) = (1.2, 1.6)$. Here, the agreement with the LES by Schneider *et al.* (2009) is again closer than with the experimental findings. At $x = 15$, shown in figure 6(d), both data sets suggest the turbulence to be more homogeneously spread over the cross-sectional area, with a peak situated in the interior of the diffuser of around 17 % of the bulk inlet velocity. The typical turbulent scales are rapidly increasing in size as soon as the separated flow in the upper right corner has become visible. In the duct, there are approximately ten adjacent streaks in the z -direction close to the wall. This persists until the diffuser throat and approximately $2h$ further downstream ($x = 2$), where this number is suddenly halved to approximately five streaks. Consequently, the typical scales are approximately twice as large in this region compared to the scales in the duct. Another $2h$ further downstream, at $x = 4$, the previously attached boundary layers are dispersed and the flow is to a larger

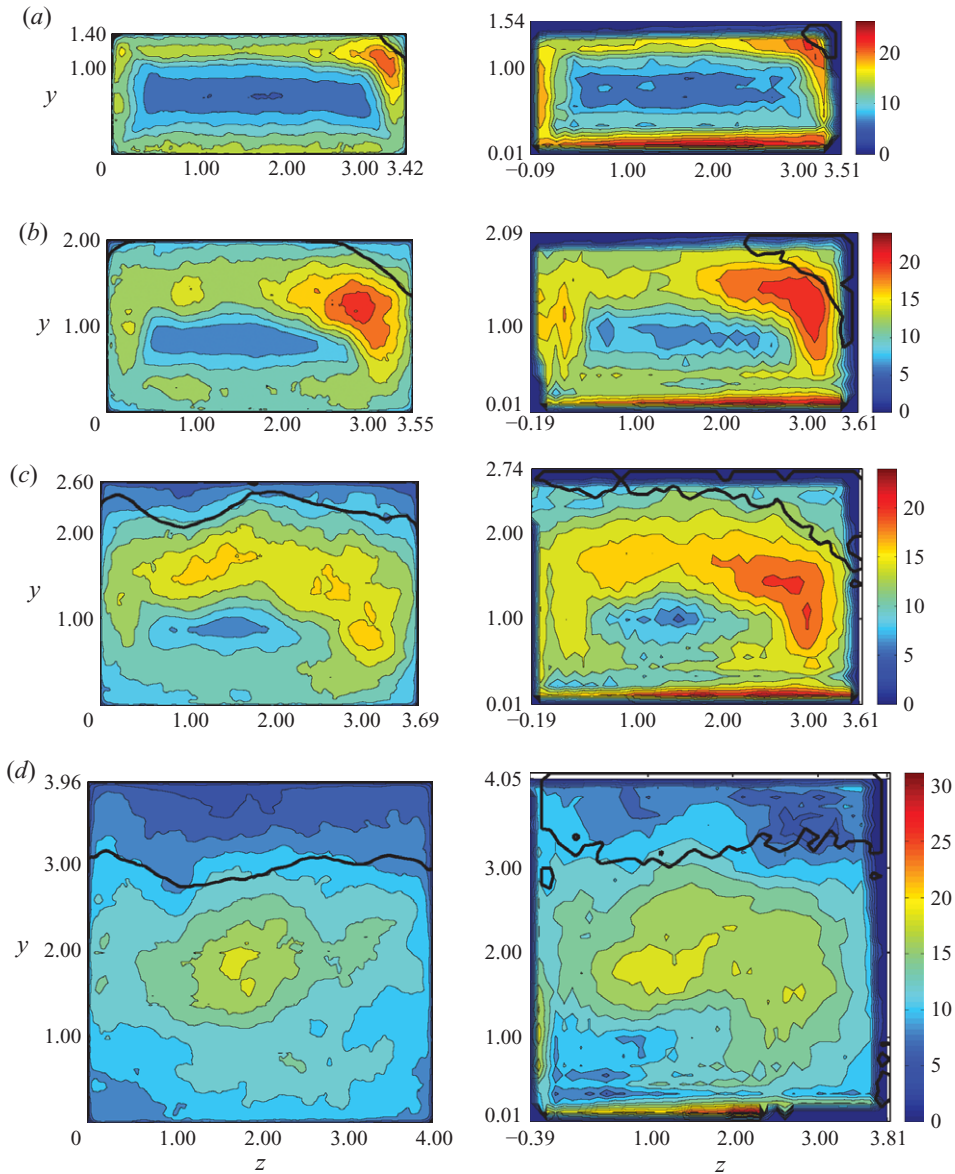


FIGURE 6. Crossflow planes of streamwise velocity fluctuations, u_{rms}/u_b 100, 2, 5, 8 and 15 h downstream of the diffuser throat. *Left*: Computation by nek5000. *Right*: Experiment by Cherry *et al.* (2008). Each streamwise position has its own colour bar on the right. Contour lines are spaced 2 u_{rms}/u_b 100 apart. Thick black lines correspond to the zero streamwise velocity contour.

extent mixed over the entire cross-section. It should be pointed out that the flow experiences a highly unsteady behaviour, characteristic of separated flow in general and enhanced by the asymmetry in the geometry in particular. Time history data shows that the fast core of the flow oscillates in one direction (i.e. y) for some time and then suddenly changes into another direction (i.e. z). More specific, the shedding of a low-velocity structure was detected in the bottom of the diffuser around $x = 14$ with a Strouhal number of $St = fh/u_b = 1/50$, i.e. at a comparably low frequency.

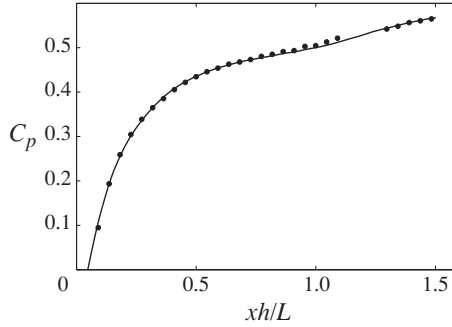


FIGURE 7. Pressure recovery coefficient relative to the pressure on the bottom wall of the diffuser inlet, where $L = 15h$ denotes the length of the diffuser. — nek5000, • experiment by Cherry *et al.* (2009).

The separated flow was found to be laminar most of the time, as opposed to the highly fluctuating flow further away from the walls, which will contribute to a highly intermittent flow in this region, both in time and space. Finally, we also compare to the pressure data (Cherry, Elkins & Eaton 2009) conducted for ‘Diffuser 1’ along the flat wall of the diffuser opposite of the top expanding wall by means of static pressure taps. The dimensionless pressure recovery coefficient, $C_p = (p - p_{ref}) / \rho u_b^2$ is plotted against the streamwise coordinate xh/L in figure 7, where p_{ref} is the reference pressure at $x = 0.045$, $L = 15h$ is the length of the diffuser, ρ is the fluid density and u_b is the bulk velocity at the inlet of the diffuser. A constant of -0.02 is added to the experimental C_p in order to facilitate the comparison. The agreement is excellent, including the rapid rise, the gradual reduction in the pressure gradient and the linear part after $x = 0.7$. This result gives important information about the quality of the computed pressure field, which plays an important role in the Reynolds stress budgets. The effective pressure rise over the diffuser computed as $\Delta C_p = C_p(xh/L = 1.48) - C_p(xh/L = 0.045)$ is $\Delta C_p^{sim} = 0.569$ for the simulation and $\Delta C_p^{exp} = 0.587$ for the experiment.

4. Conclusions

Diffuser flows are numerically hard to treat in general, not only due to their sensitivity to discretization errors, but also as a consequence of the slow, separated flow the need for long (and expensive) time integration to obtain converged turbulent statistics. Nevertheless, their importance in technical applications cannot be underestimated. Three-dimensional diffusers, in particular, are even more challenging due to the lack of statistically homogeneous directions, and hence the possibility to average over these. In this paper, we study one of the diffuser geometries (‘Diffuser 1’) experimentally investigated by Cherry *et al.* (2008). In the present set-up, special care was taken to make the present computation free from artificial inflow condition through an unsteady trip forcing and a long development section. Taking the above difficulties into account and adding the general resolution requirements of a flow at $Re = 10\,000$, the mean flow results presented here show very good agreement with experimental studies. The complex flow and the realistic Reynolds number proves that numerical simulations might qualify as a cheaper alternative to experiments. A slight discrepancy in the separated region was found, supported by findings of Schneider *et al.* (2009) and a physical explanation involving the secondary flow was

given. As the quality of the data is now assessed, the complex flow physics in the three-dimensional separation will be further investigated. In addition, as turbulence modelling in separated flows continues to be an active area of research, this data will be available as a valuable reference database, where the Reynolds stress budgets might be of particular interest.

Computer time was provided by ALCF, Argonne National Laboratory (ANL) on the IBM BG/P (ANL) and by SNIC (Swedish National Infrastructure for Computing) with a generous grant by the Knut and Alice Wallenberg (KAW) Foundation at the Centre for Parallel Computers (PDC) at the Royal Institute of Technology (KTH). The third author was supported by the US Department of Energy under contract DE-AC02-06CH11357.

REFERENCES

- BUICE, C. U. & EATON, J. K. 2000 Experimental investigation of flow through an asymmetric plane diffuser. *J. Fluids Engng* **122** (2), 433–435.
- CHERRY, E. M., ELKINS, C. J. & EATON, J. K. 2008 Geometric sensitivity of three-dimensional separated flows. *Intl J. Heat Fluid Flow* **29** (3), 803–811.
- CHERRY, E. M., ELKINS, C. J. & EATON, J. K. 2009 Pressure measurements in a three-dimensional separated diffuser. *Intl J. Heat Fluid Flow* **30** (1), 1–2.
- ELKINS, C. J., MARKL, M., PELC, N. & EATON, J. K. 2003 4D magnetic resonance velocimetry for mean velocity measurements in complex turbulent flows. *Exp. Fluids* **34**, 494–503.
- FISCHER, P. F. 1997 An overlapping Schwarz method for spectral element solution of the incompressible Navier–Stokes equations. *J. Comput. Phys.* **133** (1), 84–101.
- FISCHER, P., KRUSE, J., MULLEN, J., TUFO, H., LOTTES, J. & KERKEMEIER, S. 2008 NEK5000: Open source spectral element CFD solver. <https://nek5000.mcs.anl.gov/index.php/MainPage>.
- HERBST, A. H., SCHLATTER, P. & HENNINGSON, D. S. 2007 Simulations of turbulent flow in a plane asymmetric diffuser. *Flow Turbulence Combust.* **79**, 275–306.
- ILIESCU, T. & FISCHER, P. F. 2003 Large eddy simulation of turbulent channel flows by the rational large eddy simulation model. *Phys. Fluids* **15** (10), 3036–3047.
- JAKIRLIĆ, S., KADAVELIL, G., SIRBUBALO, E., BREUER, M., v. TERZI, D. & BORELLO, D. 2010 In *14th ERCOFTAC SIG15 Workshop on Turbulence Modelling: Turbulent Flow Separation in a three-dimensional Diffuser*. *ERCOFTAC Bulletin*. June Issue 83, case 13.2 (1). *ERCOFTAC* (in press).
- KALTENBACH, H.-J., FATICA, M., MITTAL, R., LUND, T. S. & MOIN, P. 1999 Study of flow in a planar asymmetric diffuser using large-eddy simulation. *J. Fluid Mech.* **390**, 151–185.
- LANDAHL, M. T. 1980 A note on an algebraic instability of inviscid parallel shear flow. *J. Fluid Mech.* **98** (2), 243–251.
- MADAY, Y. & PATERA, A. 1989 Spectral element methods for the Navier–Stokes equations. In *State of the Art Surveys in Computational Mechanics* (ed. A. K. Noor), pp. 71–143. ASME.
- OHLSSON, J., SCHLATTER, P., FISCHER, P. F. & HENNINGSON, D. S. 2010 Large-eddy simulation of turbulent flow in a plane asymmetric diffuser by the spectral element method. In *Direct and Large-Eddy Simulation VII* (ed. V. Armenio, B. Geurts & J. Fröhlich), Springer, to appear.
- PATERA, A. T. 1984 A spectral element method for fluid dynamics: laminar flow in a channel expansion. *J. Comput. Phys.* **54**, 468–488.
- SCHLATTER, P., ÖRLÜ, R., LI, Q., BRETHOUWER, G., FRANSSON, J. H. M., JOHANSSON, A. V., ALFREDSSON, P. H. & HENNINGSON, D. S. 2009 Turbulent boundary layers up to $Re_\theta = 2500$ studied through numerical simulation and experiments. *Phys. Fluids* **21** (5), 051702.
- SCHNEIDER, H., TERZI, D. A. & RODI, W. 2009 Reliable and accurate prediction of three-dimensional separation in asymmetric diffusers using large-eddy simulation. In *Proceedings of ASME Turbo Expo 2009: Power for Land, Sea and Air*. Orlando, Florida.
- SHERWIN, S. & KARNIADAKIS, G. 1995 A triangular spectral element method; applications to the incompressible Navier–Stokes equations. *Comput. Methods Appl. Mech. Engng* **123**, 189.

- SIMPSON, R. L. 1989 Turbulent boundary-layer separation. *Annu. Rev. Fluid Mech.* **21** (1), 205–232.
- TOMBOULIDES, A. & ORSZAG, S. 2000 Numerical investigation of transitional and weak turbulent flow past a sphere. *J. Fluid Mech.* **416**, 45–73.
- TUFO, H. M. & FISCHER, P. F. 2001 Fast parallel direct solvers for coarse grid problems. *J. Parallel Distrib. Comput.* **61** (2), 151–177.
- WASBERG, C. E., GJESDAL, T., REIF, B. A. P. & ANDREASSEN, Ø. 2009 Variational multiscale turbulence modelling in a high order spectral element method. *J. Comput. Phys.* **228** (19), 7333–7356.